

# Chemical clues on the formation of planetary systems

## C/O vs Mg/Si for HARPS GTO sample

E. Delgado Mena<sup>1,2</sup>, G. Israelian<sup>1,2</sup>, J. I. González Hernández<sup>1,2</sup>, J. C. Bond<sup>3</sup>, N. C. Santos<sup>4,5,6</sup>, S. Udry<sup>6</sup> and M. Mayor<sup>6</sup>

### ABSTRACT

Theoretical studies suggest that C/O and Mg/Si are the most important elemental ratios in determining the mineralogy of terrestrial planets. The C/O ratio controls the distribution of Si among carbide and oxide species, while Mg/Si gives information about the silicate mineralogy. We present a detailed and uniform study of C, O, Mg and Si abundances for 61 stars with detected planets and 270 stars without detected planets from the homogeneous high-quality unbiased HARPS GTO sample, together with 39 more planet-host stars from other surveys. We determine these important mineralogical ratios and investigate the nature of the possible terrestrial planets that could have formed in those planetary systems. We find mineralogical ratios quite different from those of the Sun, showing that there is a wide variety of planetary systems which are not similar to Solar System. Many of planetary host stars present a Mg/Si value lower than 1, so their planets will have a high Si content to form species such as MgSiO<sub>3</sub>. This type of composition can have important implications for planetary processes like plate tectonics, atmospheric composition or volcanism.

*Subject headings:* stars: abundances - stars: fundamental parameters - stars: planetary systems - stars: planetary systems: formation - stars: atmospheres

### 1. Introduction

The study of extrasolar planets has been a new exciting field of astrophysics for ten years now. More than 450 planets are known in 385 planetary systems. In addition, more than 80 planets out of these 450 transit their host stars and in the last few years more than 40 planets with minimum masses between 2 and 20  $M_{\oplus}$  have been discovered. The study of the photospheric stel-

lar abundances of their parent stars is the key to understand how and which of the protoplanetary clouds form planets and which do not. These studies also help us to investigate the internal and atmospheric structure and composition of extrasolar planets.

One remarkable characteristic of planet host stars is that they are considerably metal rich when compared with single field dwarfs (Gonzalez 1998; Santos et al. 2000; Gonzalez et al. 2001; Santos et al. 2001, 2004; Fischer & Valenti 2005). Two main explanations have been suggested to clarify this difference. The first of these is that the origin of this metallicity excess is primordial, so the more metals you have in the proto-planetary disk, the higher should be the probability of forming a planet. On the other hand, this excess might be produced by accretion of rocky material by the star some time after it reached the main-sequence. If pollution were the responsible for the

<sup>1</sup>Instituto de Astrofísica de Canarias, 38200 La Laguna, Tenerife, Spain: edm@iac.es

<sup>2</sup>Departamento de Astrofísica, Universidad de La Laguna, 38205 La Laguna, Tenerife, Spain

<sup>3</sup>Planetary Science Institute, 1700 E. Fort Lowell, Tucson, AZ 85719, USA

<sup>4</sup>Centro de Astrofísica, Universidade do Porto, Rua das Estrelas, 4150-762 Porto, Portugal

<sup>5</sup>Departamento de Física e Astronomia, Faculdade de Ciências, Universidade do Porto, Portugal

<sup>6</sup>Observatoire de Genève, Université de Genève, 51 Ch. des Maillettes, 1290 Sauverny, Switzerland

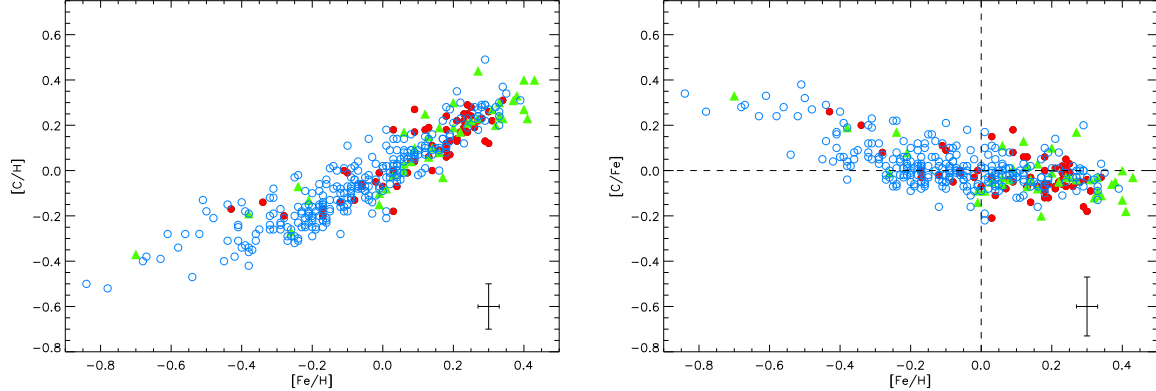


Fig. 1.—  $[C/H]$  vs  $[Fe/H]$  and  $[C/Fe]$  vs  $[Fe/H]$  for stars with (red filled circles) and without (blue open circles) detected planets from the HARPS GTO sample. Green triangles are stars with planets from other surveys.

enhanced metallicity of planet hosts, we would expect to find higher metallicities as the convective envelope mass decreases, but no such trend has been found. In addition, transit detections have shown that the mass of heavy elements in the planets appears to be correlated with the metallicity of their parent stars (Guillot et al. 2006). A recent work by Mordasini et al. (2009) finds that distributions of planetary systems are well reproduced using core-accretion models, which are dependent on dust content of the disk, thus supporting the primordial origin of supersolar metallicity in stars with planets. Recent studies on chemical abundances in stars with and without planets showed no important differences in  $[X/Fe]$  vs.  $[Fe/H]$  trends between both groups of stars (Takeda 2007; Bond et al. 2008; Neves et al. 2009; González Hernández et al. 2010). However, other works have reported less statistically significant enrichments in other species such as C, Na, Si, Ni, Ti, V, Co, Mg and Al (Gonzalez et al. 2001; Santos et al. 2000; Sadakane et al. 2002; Bodaghee et al. 2003; Fischer & Valenti 2005; Beirão et al. 2005; Gilli et al. 2006; Bond et al. 2006; Gonzalez & Laws 2007) or even important enrichments in Si and Ni (Robinson et al. 2006).

These results have important implications for models of giant planet formation and evolution. There are two major planet formation models: the core accretion model (Pollack et al. 1996), more

likely to form planets in the inner disk, and the disk instability model (Boss 1997), which is in better agreement with the conditions in the extended disk. In the first model, planets are formed by the collisional accumulation of planetesimals by a growing solid core, followed by accretion of a gaseous envelope onto the core. In the second scenario, a gravitationally unstable region in a protoplanetary disk forms self-gravitating clumps of gas and dust, within which the dust grains coagulate and sediment to form a central core (Boss 1997). In the core accretion model, planet formation is dependent on the dust content of the disk (Pollack et al. 1996) while in the disk instability model it is not (Boss 2002). Present observations are thus more compatible with core accretion model although they do not exclude disk instability.

Theoretical studies suggest that C/O and Mg/Si are the most important elemental ratios in determining the mineralogy of terrestrial planets and they can give us information about the composition of these planets. The C/O ratio controls the distribution of Si among carbide and oxide species, while Mg/Si gives information about the silicate mineralogy (Bond et al. 2010a,b). Bond et al. (2010b) carried out simulations of planet formation where the chemical composition of the protoplanetary cloud was taken as an input parameter. Terrestrial planets were found to form in all the

simulations with a wide variety of chemical compositions so these planets might be very different from the Earth. In this paper we will present C/O and Mg/Si ratios in a sample of stars with and without detected planets using new high quality spectra in order to investigate the mineralogical characteristics of those systems.

## 2. Observations

The HARPS GTO sample is composed of 451 FGK stars selected from a volume-limited stellar sample observed by the CORALIE spectrograph at La Silla observatory. These stars are slowly-rotating, non-evolved, and low-activity stars that presented no obvious radial-velocity variations at the level of the CORALIE measurement precision. For more details we point the reader to a description of the sample by Mayor et al. (2003). This sample is composed of high resolution, high signal-to-noise spectra for 71 stars with planets and 380 with no known giant planets with effective temperatures from 4500 K to 6500 K. Precise stellar parameters were taken from Sousa et al. (2008), with uncertainties of the order of 30 K for  $T_{\text{eff}}$ , 0.06 dex for  $\log g$ , 0.08 km s $^{-1}$  for  $\xi_t$  and 0.03 dex for [Fe/H]. To improve the statistics we added high quality spectroscopic observations for 42 stars hosting planets from the CORALIE survey, using the same spectral tools to determine their stellar parameters (Santos et al. 2004, 2005), and thus ensuring that the final sample is homogeneous.

## 3. Analysis

For all the elements we performed a standard LTE analysis with the 2002 revised version of the spectral synthesis code MOOG (Sneden 1973) and a grid of Kurucz ATLAS9 atmospheres with overshooting (Kurucz et al. 1993), by measuring the equivalent width (EW) of the different lines with the ARES program<sup>1</sup> (Sousa et al. 2007). All the abundances are listed in Tables 3, 4, 5, 6, 7, 8, 9, 10 and 11.

In Figs. 1, 4, 3, 5 and 6 we display at the left-bottom corner of each panel the average error bars

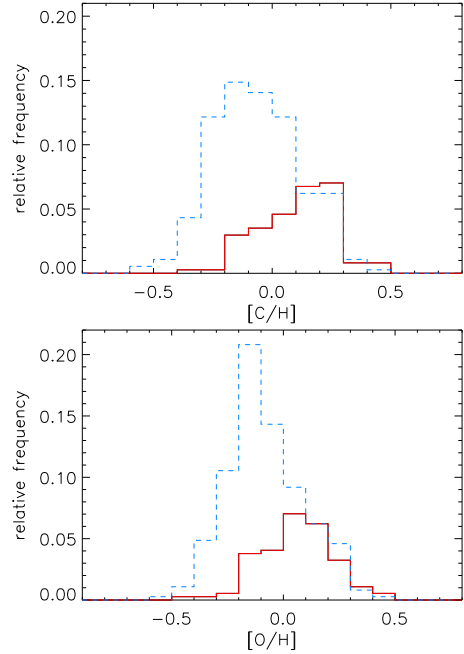


Fig. 2.— [C/H] and [O/H] distributions for stars with (red line) and without (blue dashed line) detected planets.

for the element abundances, [X/H], or abundances ratios [X/Fe].

The errors in the element abundances, [X/H], show their sensitivity to the uncertainties in the effective temperature ( $\Delta_{T_{\text{eff}}}$ ), surface gravity ( $\Delta_{\log g}$ ), microturbulence ( $\Delta_{\xi}$ ), continuum placement and the dispersion of the measurements from different spectral features ( $\Delta_{\sigma}$ ). The errors  $\Delta_{\sigma}$  were estimated as  $\Delta_{\sigma} = \sigma/\sqrt{N}$ , where  $\sigma$  is the standard deviation of the  $N$  measurements. We estimate the total error by adding in quadrature all these uncertainties.

The errors in the abundance ratios, [X/Fe], were determined taking into account the differences between the sensitivities of the resulting abundances to changes in assumed atmospheric parameters and the dispersion of the abundances from individual lines of each element.

### 3.1. Carbon

To obtain carbon abundances we used two unbleeded lines at  $\lambda$  5380.3 Å and  $\lambda$  5052.2 Å.

<sup>1</sup>The ARES code can be downloaded at <http://www.astro.up.pt/~sousasag/ares/>

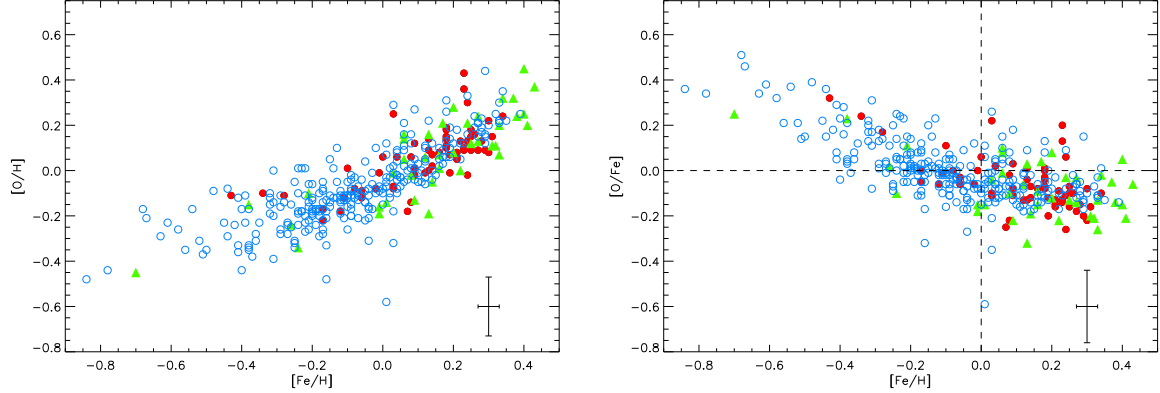


Fig. 4.—  $[O/H]$  vs  $[Fe/H]$  and  $[O/Fe]$  vs  $[Fe/H]$  for stars with (red filled circles) and without (blue open circles) detected planets from the HARPS GTO sample. Green triangles are stars with planets from other surveys.

Table 1: Atomic parameters for lines of C I, [O I] and Ni I.

Element	$\lambda$ (Å)	$\chi_l$ (eV)	$\log gf$
C I	5052.160	7.68	-1.420
C I	5380.340	7.68	-1.710
[O I]	6300.230	0.00	-9.689
Ni I	6300.399	4.27	-2.310

For the coolest stars, 5052.2 Å line becomes very weak and the abundance is calculated using only 5380.3 Å line is very high, so we removed from the samples all stars with  $T_{\text{eff}} < 5100$  K. The wavelengths and excitation energies of the lower levels were taken from VALD database (Kupka et al. 1999). The oscillator strengths,  $\log gf$  values, were adjusted using the EWs obtained from the Kurucz Solar Atlas and a solar model with  $T_{\text{eff}} = 5777$  K,  $\log g = 4.44$  and  $\xi_t = 1 \text{ km s}^{-1}$  to get  $\log \epsilon(C)_\odot = 8.56^2$  (Anders & Grevesse 1989), which is the solar value used for the differential analysis (see Table 1). We also calculated solar C abundance using a solar Harps spectrum<sup>3</sup> (daytime sky spectrum) and the same model, obtaining  $\log \epsilon(C)_\odot = 8.52$ . We note here that the spectral lines in solar spectra obtained on the daytime sky

<sup>2</sup> $\log \epsilon(X) = \log[(N(X)/N(H)] + 12$

<sup>3</sup>The HARPS solar spectra can be downloaded at <http://www.eso.org/sci/facilities/lasilla/instruments/harps//inst/monitoring/sun.html>

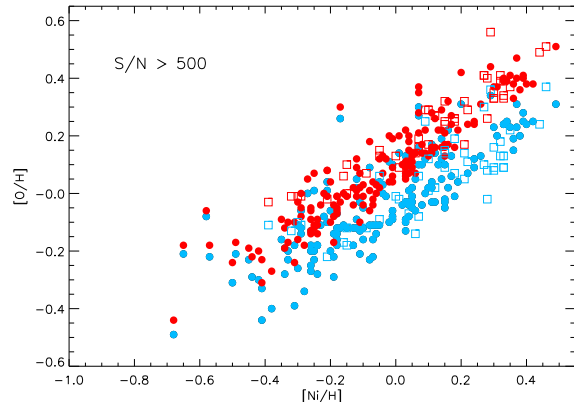


Fig. 3.—  $[O/H]$  vs  $[Ni/H]$  for stars with (squares) and without (circles) detected planets from the HARPS GTO sample. Red and blue symbols correspond to O abundance with and without the contribution of Ni, respectively.

are known to exhibit EW and line depth changes (e.g. Gray et al. 2000). This may explain these different C abundances. We may refer to the work by González Hernández et al. (2010) to see the differences in element abundances from slightly different solar HARPS spectra and those of the solar ATLAS spectrum. In this work we will use ATLAS solar values as reference values. However, we will plot both solar values in the C/O vs Mg/Si figure (see Figs. 8 and 9).

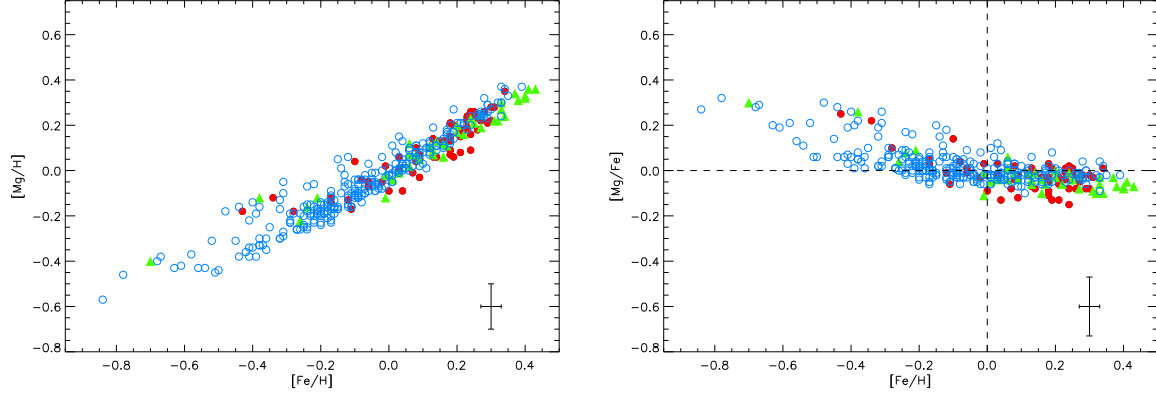


Fig. 5.—  $[\text{Mg}/\text{H}]$  vs  $[\text{Fe}/\text{H}]$  and  $[\text{Mg}/\text{Fe}]$  vs  $[\text{Fe}/\text{H}]$  for stars with (red filled circles) and without (blue open circles) detected planets from the HARPS GTO sample. Green triangles are stars with planets from other surveys.

In Fig. 1 we show the  $[\text{C}/\text{H}]$  and  $[\text{C}/\text{Fe}]$  ratios as a function of  $[\text{Fe}/\text{H}]$ . The samples of stars both with and without detected planets behave quite similarly, although there is an average overabundance of about 0.15 dex in the total planet-host stars with respect to the comparison sample ( $\langle [\text{C}/\text{H}] \rangle_P = 0.10$ ,  $\sigma = 0.16$ , RMS = 0.19 and  $\langle [\text{C}/\text{H}] \rangle_C = -0.06$ ,  $\sigma = 0.18$ , RMS = 0.19). Since targets with planets are on average more metal-rich than the stars of comparison sample, their abundance distributions correspond to the extensions of the comparison sample trends at high metallicity (see Fig. 2). Such a trend supports the primordial scenario as an explanation of the overmetallicity of planet-host stars. C abundances present a bimodality for metallicities lower than solar, due to the average overabundance of thick disc stars in comparison with the thin disk stars (see Neves et al. 2009).  $[\text{C}/\text{Fe}]$  clearly decreases with  $[\text{Fe}/\text{H}]$  in the metallicity range  $-0.8 < [\text{Fe}/\text{H}] < -0.2$ , but for higher metallicities this ratio is more flattened. This flattening of the  $[\text{C}/\text{Fe}]$  ratios was also found by other authors (e.g. Sadakane et al. 2002) but in other works a monotonic decrease of  $[\text{C}/\text{Fe}]$  with metallicity was reported (e.g. Andersson & Edvardsson 1994; Ecuvillon et al. 2006). Since we do not observe differences between the samples with and without detected planets, this behaviour must be evidence of the chemical evolution of the Galactic disk.

### 3.2. Oxygen

There are several indicators to measure oxygen abundances: the near-IR OI triplet at  $\lambda 7771.5$  Å, the forbidden lines of  $[\text{O I}]$  at  $\lambda 6300$  Å and  $\lambda 6363$  Å and the near-UV OH lines at  $\lambda 3100$  Å. Ecuvillon et al. (2006) made a comparative study of the three indicators in a sample of stars with and without detected planets and found good agreement between the  $[\text{O}/\text{H}]$  ratios from forbidden and OH lines, while the NLTE triplet shows a systematically lower abundance. Unfortunately, only forbidden line is available in HARPS spectra, so we used this indicator to obtain oxygen LTE abundances, since it is well known that this indicator is not significantly affected by deviations from LTE (e.g. Kiselman 1991).

The spectral region around this feature has telluric lines which can be blended with the  $[\text{O I}]$  line in some stars. So we made a detailed observation of the spectra to remove these objects from the sample in order to avoid wrong values of the O abundance. This, together with the limitation on  $T_{\text{eff}}$ , makes a final sample of 69 and 270 stars with and without detected planets from HARPS, and 31 stars with planets from other surveys. This line is also blended with a Ni I absorption at  $\lambda 6300.399$  Å (Lambert 1978; Allende Prieto et al. 2001), so we estimated the EW of the Ni line us-

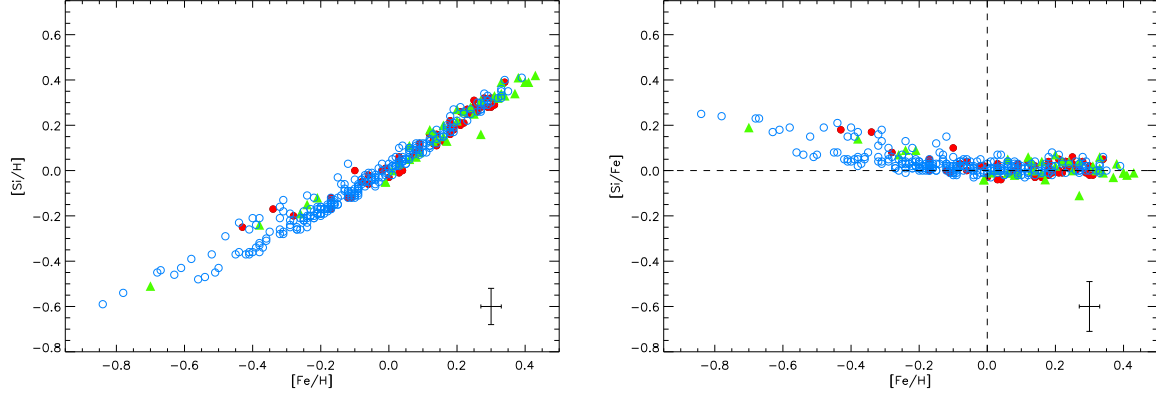


Fig. 6.—  $[\text{Si}/\text{H}]$  vs  $[\text{Fe}/\text{H}]$  and  $[\text{Si}/\text{Fe}]$  vs  $[\text{Fe}/\text{H}]$  for stars with (red filled circles) and without (blue open circles) detected planets from the HARPS GTO sample. Green triangles are stars with planets from other surveys.

ing the `ewfind` driver of MOOG (Sneden 1973). Ni abundances for HARPS stars were taken from Neves et al. (2009). For the additional sample stars we calculate Ni abundances in the same way as in Neves et al. (2009). The oxygen contribution has been obtained by subtracting the Ni EW from the measured EW of whole 6300.23 Å feature. The wavelengths, excitation energies of the lower levels and oscillator strengths of the Ni I absorption were taken from Allende Prieto et al. (2001), while the adopted atomic data for [O I] are from Lambert (1978). The  $\log g_f$  value of the [O I] line was slightly modified in order to obtain  $\log \epsilon(\text{O})_{\odot} = 8.74$  (Nissen et al. 2002), which is the solar value used for the differential analysis (see Table 1). We also calculated solar O abundance using the solar Harp spectrum (daytime sky spectrum) and the same model we used in Sect. 3.1, obtaining  $\log \epsilon(\text{O})_{\odot} = 8.60$ , a quite lower value. In Fig. 3 we can see the effect of Ni in oxygen abundances which becomes greater for higher Ni abundances, as we might expect.

In Fig. 4 we show the  $[\text{O}/\text{H}]$  and  $[\text{O}/\text{Fe}]$  ratios as a function of  $[\text{Fe}/\text{H}]$ . There appear to be no clear differences between stars with and without detected planets. This result is in disagreement with Si enrichment in stars with planets with respect to stars without known planets found by Robinson et al. (2006), since they would also expect to find an O enrichment in

these stars. However, there is an average overabundance of about 0.13 dex in the planet hosts with respect to the comparison sample ( $\langle [\text{O}/\text{H}] \rangle_P = 0.05$ ,  $\sigma = 0.16$ , RMS = 0.17 and  $\langle [\text{O}/\text{H}] \rangle_C = -0.08$ ,  $\sigma = 0.17$ , RMS = 0.19). As mentioned in Sect. 3.1, the abundance distributions of stars with planets correspond to the extensions of the comparison sample trends at high  $[\text{Fe}/\text{H}]$  (see Fig. 2).  $[\text{O}/\text{Fe}]$  clearly decreases with  $[\text{Fe}/\text{H}]$  in the metallicity range  $-0.8 < [\text{Fe}/\text{H}] < 0.0$ , although this fall is not so steep. This behaviour has been also reported in previous works (Bensby et al. 2004; Ecuvillon et al. 2006), where  $[\text{O}/\text{Fe}]$  showed a monotonic decrease with metallicity, in agreement with galactic evolution models.

### 3.3. Magnesium and Silicon

Mg and Si abundances were calculated using the line list of Neves et al. (2009), adding a Mg line at  $\lambda 6318.72$  Å. Solar values that we used for the differential analysis of the two elements are  $\log \epsilon(\text{Mg})_{\odot} = 7.58$  and  $\log \epsilon(\text{Si})_{\odot} = 7.55$  (Anders & Grevesse 1989). The abundance values obtained from the Harps 1000 spectrum (daytime sky spectrum) are  $\log \epsilon(\text{Mg})_{\odot} = 7.54$  and  $\log \epsilon(\text{Si})_{\odot} = 7.52$ , slightly lower than the reference values.

In Fig. 6 we can see  $[\text{Si}/\text{H}]$  and  $[\text{Si}/\text{Fe}]$  as a function of  $[\text{Fe}/\text{H}]$ . Robinson et al. (2006) found clear and significant overabundances of Si in stars

with planets with respect to comparison stars. On the other hand Gonzalez & Laws (2007) reported systematically lower abundances of this element in the higher metallicity range for stars with planets. However, and in agreement with recent works (Neves et al. 2009; González Hernández et al. 2010), we do not find significant differences between the stars with and without detected planets although the average values are 0.19 dex greater in stars hosting planets ( $\langle \text{[Si/H]} \rangle_P = 0.14$ ,  $\sigma = 0.17$ , RMS = 0.22 and  $\langle \text{[Si/H]} \rangle_C = -0.05$ ,  $\sigma = 0.19$ , RMS = 0.20), again due to the higher metallicity of the planet-host sample. For  $[\text{Mg}/\text{H}]$  there is a similar effect, owing to the same reason ( $\langle \text{[Mg/H]} \rangle_P = 0.10$ ,  $\sigma = 0.15$ , RMS = 0.18 and  $\langle \text{[Mg/H]} \rangle_C = -0.06$ ,  $\sigma = 0.18$ , RMS = 0.19). At subsolar metallicities all stars present high Mg abundances irrespective of  $T_{\text{eff}}$ . However, this is not the case for  $[\text{Fe}/\text{H}] \geq 0$ , where stars without detected planets have higher Mg abundances,  $\langle \text{[Mg/Fe]} \rangle_P = -0.040$ ,  $\sigma = 0.04$ , RMS = 0.06 and  $\langle \text{[Mg/Fe]} \rangle_C = -0.014$ ,  $\sigma = 0.04$ , RMS = 0.04 (see Fig. 5), also for different temperatures. Nevertheless, this effect disappears when we take into account only solar analogs, with  $5600 < T_{\text{eff}} < 5950$  K, perhaps due to the low number of stars with planets in this group. Therefore, it might be an effect in Mg abundances due to the presence of planetary companions (see Fig. 7). For both elements we observe the same bimodality we found for C abundances at lower metallicities, owing to the different populations from thin and thick disk (Neves et al. 2009).  $[\text{Mg/Fe}]$  and  $[\text{Si/Fe}]$  ratios show a decrease for  $[\text{Fe}/\text{H}] < 0$  but they flatten for higher metallicities as a consequence of the chemical evolution of the Galaxy.

#### 4. C/O vs Mg/Si

In Fig. 8, C/O ratios as a function of Mg/Si are presented for different temperature ranges. These ratios are calculated as:

$$A/B = N_A/N_B = 10^{\log \epsilon(A)} / 10^{\log \epsilon(B)} \quad (1)$$

where  $\log \epsilon(A)$  and  $\log \epsilon(B)$  are the absolute abundances, so they are not dependent on solar reference abundances. In our sample, 34% of stars with known planets have C/O values greater than 0.8, which means that Si will exist primarily as SiC

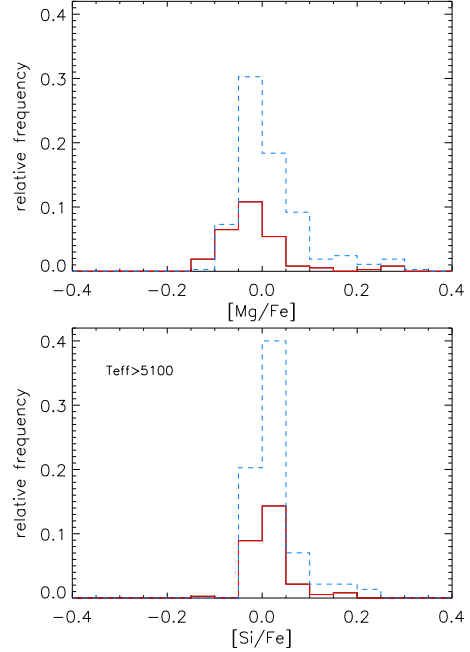


Fig. 7.—  $[\text{Si/Fe}]$  and  $[\text{Mg/Fe}]$  distributions for stars with (red line) and without (blue dashed line) detected planets.

(see Sect. 4.1). On the other hand, 66% of stars with known planets have C/O values lower than 0.8 and Si will be present in rock-forming minerals as the  $\text{SiO}_2$  structural unit. In these cases, silicate mineralogy will be controlled by Mg/Si ratio. 52% of these stars (with  $\text{C/O} < 0.8$ ) present Mg/Si ratios between 1 and 2, similar to the solar ratio, while 48% have ratios lower than 1. We do not find any star with  $\text{Mg/Si} > 2$ . If we take into account all stars, irrespective of their C/O value, these percentages are similar (see Table 2).

Comparison sample stars are shifted towards higher Mg/Si ratios (see Fig. 9), since they present higher Mg abundances as mentioned in Sect. 3.3. We do not find any significant effect related to the effective temperature of the stars (see Fig. 9). Both Atlas and Harps solar ratios are represented in the plots. Mg/Si ratios are equal for both spectra although C/O ratio is a little greater for Harps spectrum. In any case, this value is in the lowest limit of C-rich systems.

Table 2: C/O and Mg/Si distributions for stars with planets

Ratio	Percentage	Principal Composition
C/O > 0.8	34%	graphite, TiC and solid Si as SiC
C/O < 0.8	66%	solid Si as $\text{SiO}_4^{4-}$ or $\text{SiO}_2$
Mg/Si < 1	56%	pyroxene, metallic Fe and excess Si as feldspars
1 < Mg/Si < 2	44%	equal pyroxene and olivine
Mg/Si > 2	0%	olivine and excess Mg as $\text{MgO}$

The errors in the abundance ratios C/O and Mg/Si were estimated by evaluating an increase or a decrease in the  $\log \epsilon(A) - \log \epsilon(B)$  abundance ratio, due to the relative error, using the Eq. 1.

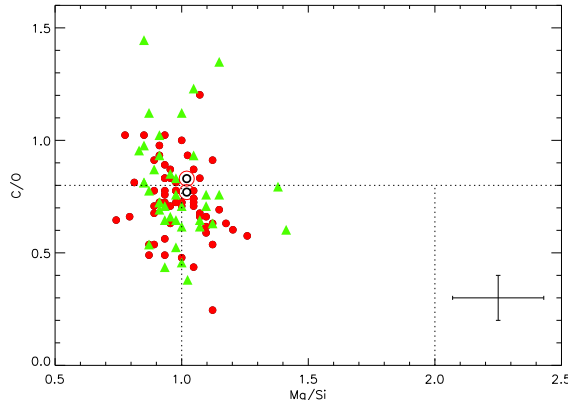


Fig. 8.— C/O vs Mg/Si for stars with planets from the HARPS GTO sample (red filled circles). Green triangles are stars with planets from other surveys.

#### 4.1. Terrestrial Planet Compositions

The wide variety of host star compositions determined in this study will presumably result in a diverse range of compositions of solid material available for terrestrial planet formation. As previously discussed by Bond et al. (2010b), under the assumption of equilibrium those systems with a C/O value above 0.8 will contain carbide-rich phases (such as graphite, SiC and TiC) in the innermost regions of the disk. Metallic Fe and Mg

silicates such as olivine ( $\text{Mg}_2\text{SiO}_4$ ) and pyroxene ( $\text{MgSiO}_3$ ) are also present and are located further from the host star. Terrestrial planets forming in these planetary systems are expected to be C-rich, containing significant amounts of C in addition to Si, Fe, Mg and O.

For systems with a C/O value below 0.8, Si will be present in the solid form primarily as  $\text{SiO}_4^{4-}$  or  $\text{SiO}_2$ , predominantly forming Mg-silicates. The exact composition of the Mg-silicates is controlled by the Mg/Si value. For systems with a Mg/Si value between 1 and 2, the silicates present are predominately olivine and pyroxene in a condensation sequence closely resembling Solar. This is expected to result in the production of terrestrial planets similar in composition to that of Earth (in that their composition will be dominated by O, Fe, Mg and Si, with small amounts of Ca and Al also present).

However, 56% of all planetary host stars in this study have a Mg/Si value less than 1. For such a composition, the solid component of the disk is dominated by approximately equal amounts of pyroxene and metallic Fe with minimal amounts of olivine present. Feldspars are also likely to be present as all available Mg is partitioned into pyroxene, leaving excess Si available to form other silicate species. This is expected to result in the production of terrestrial planets that can be best described as being Si-rich Earths. They will still be dominated by O, Fe, Mg and Si and contain minor amounts of other elements such as Ca and Al. However, their bulk Si content is expected to be well above any value previously observed for a planetary body. Note that for this study, the high-Si planetary compositions are due to the fact that there is an excess of Si compared to Mg within the disk system and does not necessarily imply an el-

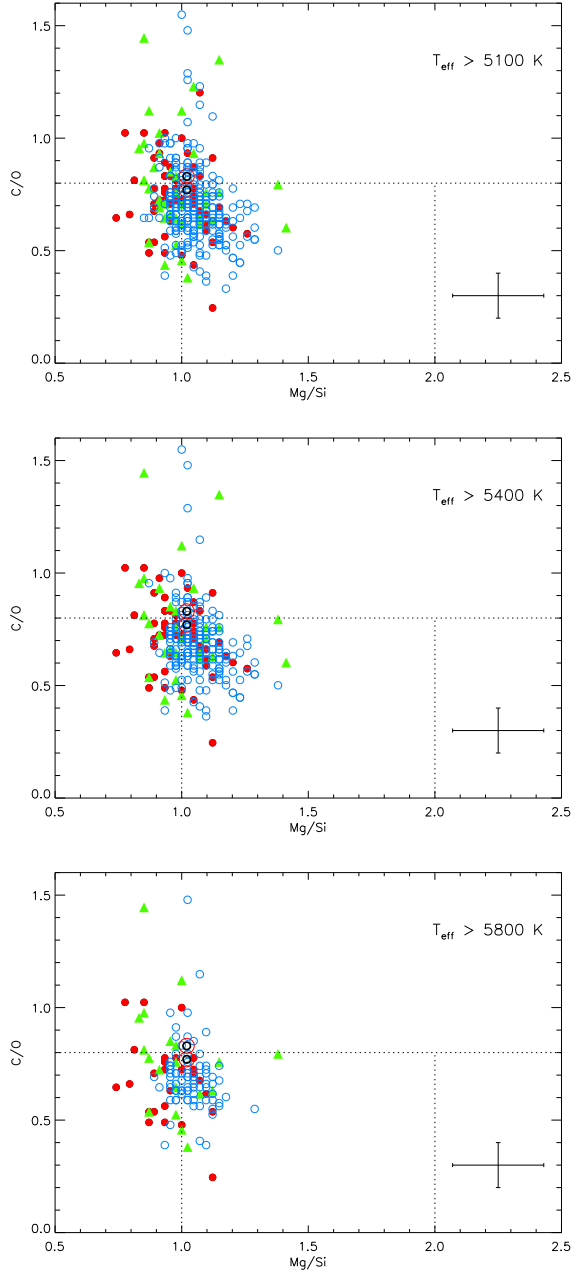


Fig. 9.— C/O vs Mg/Si for stars with (red filled circles) and without (blue open circles) detected planets from the HARPS GTO sample. Green triangles are stars with planets from other surveys.

elevated Si abundance. Such an elevated Si content is predicted to produce a quartz-feldspar rich terrestrial planet with a composition more like that

of Earth's continental crust material than that of Earth's olivine-dominated mantle. A composition such as this can have drastic implications for planetary processes such as plate tectonics and atmospheric composition. For example, volcanism on a Si-rich planet is expected to be intermediate to felsic in composition (i.e. >52% silica by weight) due to the potentially high SiO<sub>2</sub> content of the planet itself, producing igneous species such as andesite, rhyolite and granite. Eruptions may also be more explosive in nature due to the high viscosity of SiO<sub>2</sub>-rich magma trapping volatiles within the magma. On Earth, such eruptions are commonly observed at convergent tectonic plate margins (i.e. subduction zones) (for intermediate compositions) and above intra-plate hot spots (for felsic compositions). Mount Pinatubo is a well-known example of an intermediate composition volcano while the Long Valley Caldera in CA, USA, is an example of a felsic eruption. Although the full implications of the compositional variations described here still require detailed study, it is clear that a diverse range of terrestrial planets are likely to exist in extrasolar planetary systems.

#### 4.2. Planet Formation

It has been previously suggested (e.g. Bond et al. 2010b) that planetary systems with C/O values above 0.8 may possess an alternative mass distribution profile for solid material, potentially making it easier either for giant planets to form closer to the host star than previously expected or for terrestrial planets to form in the inner regions of the disk. However, we find no evidence of any trends with C/O values for either planetary period, semi-major axis or mass (see Fig. 10). As such, it appears that any effects of an alternative solid mass distribution due to high concentrations of refractory C-rich material are not preserved in the architecture of the system. This is believed to be due to the fact that Bond et al. (2010b) only considered equilibrium-driven condensation and did not include the effects of disequilibrium or the migration and radial mixing of material within the disk. Simulations addressing this issue are in progress. It should be noted, however, that we are still only able to detect giant planets. This conclusion may not hold for extrasolar terrestrial planets which require significantly smaller amounts of solid material.

## 5. Conclusions

We present a detailed study of C, O, Mg and Si abundances for a sample of 100 and 270 stars with and without known giant planets with effective temperatures between 5100 K and 6500 K, with the aim of studying the mineralogical composition of terrestrial planets that could have formed in those systems.

We do not observe any special difference between abundances of stars with and without detected planets for C, O and Si. However, we find higher Mg abundances for stars without detected planets making the Mg/Si ratio greater in those stars. This effect is not so clear for solar analogs but the number of stars is not large enough to discard a possible effect due to the presence of planets.

C/O and Mg/Si ratios were obtained to study the mineralogy the possible planets that could have formed around these stars. 34% of stars with known planets have C/O values greater than 0.8, so there is a big fraction of C-rich systems, very different from our Solar System. On the other hand, 56% of stars with known planets present Mg/Si values lower than 1, so these systems are more probably to host Si-rich earths, with a Si excess much greater than any value previously observed for a planetary body. This can have extreme implications for processes as plate tectonics or volcanism. We also found stars very similar to our Sun but it is clear that a wide variety of planets will probably exist within extrasolar planetary systems.

E.D.M, J.I.G.H. and G.I. would like to thank financial support from the Spanish Ministry project MICINN AYA2008-04874. J.I.G.H. acknowledges financial support from the Spanish Ministry project MICINN AYA2008-00695 and also from the Spanish Ministry of Science and Innovation (MICINN) under the 2009 Juan de la Cierva Programme.

N.C.S. would like to thank the support by the European Research Council/European Commu-

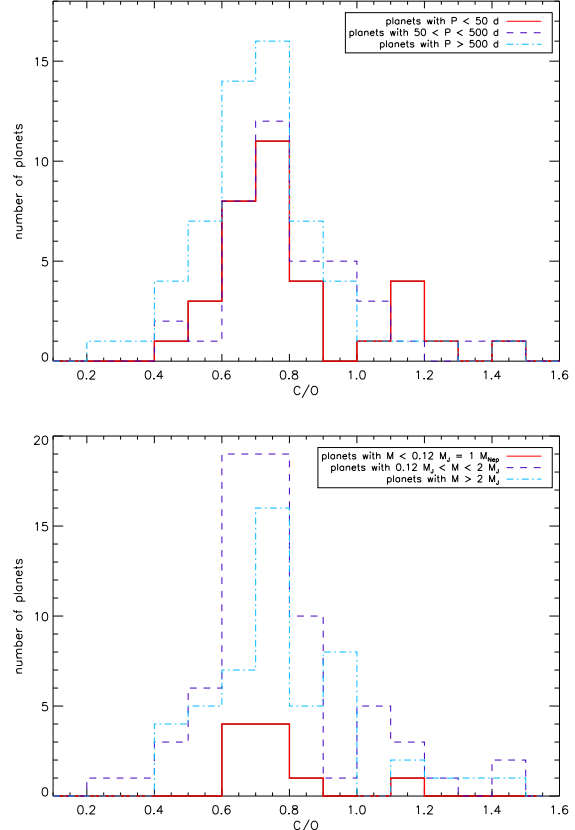


Fig. 10.— C/O distributions of planet host stars for different period and mass ranges of their companions.

nity under the FP7 through a Starting Grant, as well from Fundação para a Ciéncia e a Tecnologia (FCT), Portugal, through a Ciéncia 2007 contract funded by FCT/MCTES (Portugal) and POPH/FSE (EC), and in the form of grant reference PTDC/CTE-AST/098528/2008 from FCT/MCTES.

This work has also made use of the IRAF facility, and the Encyclopaedia of extrasolar planets.

## A. Appendix material

Table 3: Stars with planets from the HARPS GTO survey.

Star	T <sub>eff</sub> K	log g km s <sup>-1</sup>	$\xi_t$ km s <sup>-1</sup>	[Fe/H]	[O/H]	[Ni/H]	[C/H]	[Mg/H]	[Si/H]	C/O	Mg/Si
HD142	6403.	4.62	1.74	0.09	-0.02	0.01	0.17	-0.03	0.11	1.02	0.78
HD1237	5514.	4.50	1.09	0.07	-0.18	0.06	-0.01	-0.01	0.06	0.98	0.91
HD2638	5198.	4.43	0.74	0.12	-0.01	0.15	0.18	0.10	0.16	1.02	0.93
HD4308	5644.	4.38	0.90	-0.34	-0.10	-0.30	-0.14	-0.12	-0.17	0.60	1.20
HD10647	6218.	4.62	1.22	0.00	0.06	-0.05	-0.07	-0.09	-0.03	0.49	0.93
HD11964A	5332.	3.90	0.99	0.08	0.06	0.07	0.04	0.10	0.08	0.63	1.12
HD16141	5806.	4.19	1.11	0.16	0.08	0.15	0.09	0.13	0.13	0.68	1.07
HD16417	5841.	4.16	1.18	0.13	0.09	0.15	0.06	0.14	0.13	0.62	1.10
HD17051	6227.	4.53	1.29	0.19	0.07	0.18	0.07	0.06	0.19	0.66	0.79
HD19994	6289.	4.48	1.72	0.24	0.30	0.27	0.29	0.09	0.25	0.65	0.74
HD20782	5774.	4.37	1.00	-0.06	-0.12	-0.09	-0.07	-0.07	-0.06	0.74	1.05
HD22049	5153.	4.53	0.90	-0.11	-0.12	-0.15	0.00	-0.17	-0.12	0.87	0.95
HD23079	5980.	4.48	1.12	-0.12	-0.18	-0.15	-0.14	-0.13	-0.12	0.72	1.05
HD28185	5667.	4.42	0.94	0.21	0.08	0.28	0.22	0.18	0.26	0.91	0.89
HD39091	6003.	4.42	1.12	0.09	0.01	0.10	0.04	0.07	0.08	0.71	1.05
HD45364	5434.	4.38	0.71	-0.17	-0.17	-0.16	-0.17	-0.12	-0.12	0.66	1.07
HD47186	5675.	4.36	0.93	0.23	0.09	0.30	0.19	0.22	0.27	0.83	0.95
HD52265	6136.	4.36	1.32	0.21	0.06	0.22	0.13	0.15	0.21	0.78	0.93
HD65216	5612.	4.44	0.78	-0.17	-0.22	-0.21	-0.20	-0.14	-0.17	0.69	1.15
HD66428	5705.	4.31	0.96	0.25	0.09	0.32	0.24	0.26	0.28	0.93	1.02
HD69830	5402.	4.40	0.80	-0.06	-0.09	-0.05	-0.06	-0.05	-0.02	0.71	1.00
HD70642	5668.	4.40	0.82	0.18	0.10	0.23	0.11	0.14	0.22	0.68	0.89
HD73256	5526.	4.42	1.11	0.23	0.10	0.27	0.17	0.19	0.27	0.78	0.89
HD75289	6161.	4.37	1.29	0.30	0.08	0.30	0.12	0.22	0.28	0.72	0.93
HD82943	5989.	4.43	1.10	0.26	0.16	0.30	0.19	0.18	0.26	0.71	0.89
HD83443	5511.	4.43	0.93	0.34	0.24	0.44	0.31	0.35	0.39	0.78	0.98
HD92788	5744.	4.39	0.95	0.27	0.09	0.33	0.22	0.22	0.28	0.89	0.93
HD93083	5105.	4.43	0.94	0.09	0.12	0.10	0.27	0.05	0.12	0.93	0.91
HD100777	5536.	4.33	0.81	0.25	0.15	0.32	0.24	0.23	0.27	0.81	0.98
HD101930	5164.	4.40	0.91	0.13	0.14	0.15	0.19	0.14	0.15	0.74	1.05
HD102117	5657.	4.31	0.99	0.28	0.13	0.33	0.23	0.26	0.32	0.83	0.93
HD107148	5805.	4.40	0.93	0.31	0.15	0.38	0.22	0.28	0.29	0.78	1.05
HD108147	6260.	4.47	1.30	0.18	0.15	0.15	0.06	0.07	0.16	0.54	0.87
HD111232	5460.	4.43	0.62	-0.43	-0.11	-0.39	-0.17	-0.18	-0.25	0.58	1.26
HD114729	5844.	4.19	1.23	-0.28	-0.11	-0.29	-0.20	-0.18	-0.20	0.54	1.12
HD114783	5133.	4.42	0.88	0.03	-0.08	0.07	0.18	0.06	0.06	1.20	1.07
HD117207	5667.	4.32	1.01	0.22	0.13	0.24	0.17	0.18	0.21	0.72	1.00
HD117618	5990.	4.41	1.13	0.03	-0.07	0.04	0.00	0.01	0.05	0.78	0.98
HD121504	6022.	4.49	1.12	0.14	0.02	0.12	0.00	0.06	0.11	0.63	0.95
HD130322	5365.	4.37	0.90	-0.02	-0.08	-0.02	-0.05	-0.05	0.00	0.71	0.95
HD134987	5740.	4.30	1.08	0.25	0.18	0.32	0.28	0.25	0.31	0.83	0.93
HD141937	5893.	4.45	1.00	0.13	0.00	0.12	0.06	0.06	0.12	0.76	0.93
HD142022A	5508.	4.35	0.83	0.19	-0.01	0.20	0.13	0.20	0.18	0.91	1.12

Table 4: Stars with planets from the HARPS GTO survey.

Star	T <sub>eff</sub> K	log <i>g</i>	$\xi_t$ km s <sup>-1</sup>	[Fe/H]	[O/H]	[Ni/H]	[C/H]	[Mg/H]	[Si/H]	C/O	Mg/Si
HD147513	5858.	4.50	1.03	0.03	0.25	0.09	-0.18	0.01	-0.01	0.25	1.12
HD159868	5558.	3.96	1.02	-0.08	-0.08	-0.09	-0.13	-0.04	-0.05	0.59	1.10
HD160691	5780.	4.27	1.09	0.30	0.22	0.35	0.26	0.28	0.32	0.72	0.98
HD168746	5568.	4.33	0.81	-0.10	0.01	-0.08	-0.01	0.04	0.00	0.63	1.17
HD169830	6361.	4.21	1.56	0.18	0.19	0.18	0.12	0.13	0.19	0.56	0.93
HD179949	6287.	4.54	1.36	0.21	0.05	0.21	0.14	0.08	0.20	0.81	0.81
HD190647	5639.	4.18	0.99	0.23	0.43	0.27	0.25	0.24	0.25	0.44	1.05
HD196050	5917.	4.32	1.21	0.23	0.36	0.29	0.22	0.23	0.26	0.48	1.00
HD202206	5757.	4.47	1.01	0.29	0.09	0.33	0.13	0.21	0.28	0.72	0.91
HD204313	5776.	4.38	1.00	0.18	0.11	0.22	0.18	0.15	0.19	0.78	0.98
HD208487	6146.	4.48	1.24	0.08	-0.14	0.06	0.04	0.04	0.07	1.00	1.00
HD210277	5505.	4.30	0.86	0.18	0.14	0.21	0.24	0.21	0.21	0.83	1.07
HD212301	6271.	4.55	1.29	0.18	0.18	0.19	0.09	0.09	0.17	0.54	0.89
HD213240	5982.	4.27	1.25	0.14	0.07	0.16	0.11	0.13	0.16	0.72	1.00
HD216435	6008.	4.20	1.34	0.24	-0.02	0.28	0.17	0.16	0.26	1.02	0.85
HD216770	5424.	4.38	0.91	0.24	0.13	0.32	0.25	0.26	0.27	0.87	1.05
HD221287	6374.	4.62	1.29	0.04	0.06	-0.02	-0.07	-0.09	0.00	0.49	0.87
HD222582	5779.	4.37	1.00	-0.01	-0.01	0.00	-0.01	0.02	0.01	0.66	1.10

Table 5: Stars with planets from other surveys.

Star	T <sub>eff</sub> K	log g km s <sup>-1</sup>	$\xi_t$	[Fe/H]	[O/H]	[Ni/H]	[C/H]	[Mg/H]	[Si/H]	C/O	Mg/Si
HD2039	5976	4.45	1.26	0.32	0.11	0.35	0.20	0.22	0.32	0.81	0.85
HD3651	5173	4.37	0.74	0.12	0.06	0.15	0.25	0.11	0.18	1.02	0.91
HD4203	5636	4.23	1.12	0.40	0.25	0.42	0.40	0.32	0.39	0.93	0.91
HD8574	6151	4.51	1.45	0.06	0.16	0.04	0.00	0.02	0.05	0.46	1.00
HD9826	6212	4.26	1.69	0.13	-0.19	0.09	0.15	0.07	0.17	1.45	0.85
HD10697	5641	4.05	1.13	0.14	-0.05	0.13	0.10	0.13	0.14	0.93	1.05
HD13445	5163	4.52	0.72	-0.24	-0.34	-0.26	-0.07	-0.16	-0.15	1.23	1.05
HD20367	6138	4.53	1.22	0.17	0.21	0.07	-0.03	0.11	0.13	0.38	1.02
HD23596	6108	4.25	1.30	0.31	0.11	0.35	0.27	0.22	0.33	0.95	0.83
HD30177	5588	4.29	1.08	0.38	0.24	0.42	0.33	0.31	0.41	0.81	0.85
HD37124	5546	4.50	0.80	-0.38	-0.15	-0.39	-0.19	-0.12	-0.24	0.60	1.41
HD38529	5674	3.94	1.38	0.40	0.45	0.42	0.27	0.33	0.39	0.44	0.93
HD41004	5242	4.35	1.01	0.16	0.07	0.16	0.19	0.12	0.20	0.87	0.89
HD46375	5268	4.41	0.97	0.20	0.28	0.26	0.30	0.20	0.27	0.69	0.91
HD50554	6026	4.41	1.11	0.01	-0.14	-0.04	-0.08	-0.04	0.00	0.76	0.98
HD72659	5995	4.30	1.42	0.03	-0.01	0.01	-0.02	-0.01	0.03	0.65	0.98
HD73526	5699	4.27	1.26	0.27	0.24	0.27	0.23	0.25	0.31	0.65	0.93
HD74156	6112	4.34	1.38	0.16	0.01	0.15	0.08	0.06	0.15	0.78	0.87
HD75732	5279	4.37	0.98	0.33	0.07	0.39	0.30	0.30	0.39	1.12	0.87
HD76700	5737	4.25	1.18	0.41	0.20	0.40	0.23	0.36	0.39	0.71	1.00
HD89744	6234	3.98	1.62	0.22	0.00	0.17	0.17	0.16	0.26	0.98	0.85
HD95128	5954	4.44	1.30	0.06	0.05	0.07	0.03	0.07	0.05	0.63	1.12
HD106252	5899	4.34	1.08	-0.01	-0.16	-0.07	-0.10	-0.02	-0.05	0.76	1.15
HD114762	5884	4.22	1.31	-0.70	-0.45	-0.73	-0.37	-0.40	-0.51	0.79	1.38
HD143761	5853	4.41	1.35	-0.21	-0.10	-0.22	-0.13	-0.12	-0.12	0.62	1.07
HD145675	5311	4.42	0.92	0.43	0.37	0.45	0.40	0.36	0.42	0.71	0.93
HD150706	5961	4.50	1.11	-0.01	-0.19	-0.10	-0.15	-0.12	-0.05	0.72	0.91
HD168443	5617	4.22	1.21	0.06	0.14	0.08	0.17	0.12	0.11	0.71	1.10
HD178911B	5600	4.44	0.95	0.27	0.13	0.28	0.44	0.19	0.16	1.35	1.15
HD183263	5991	4.38	1.23	0.34	0.32	0.37	0.23	0.24	0.33	0.54	0.87
HD186427	5772	4.40	1.07	0.08	-0.02	0.08	0.04	0.07	0.06	0.76	1.10
HD187123	5845	4.42	1.10	0.13	0.16	0.13	0.06	0.09	0.13	0.52	0.98
HD190228	5327	3.90	1.11	-0.26	-0.24	-0.28	-0.27	-0.22	-0.19	0.62	1.00
HD190360A	5584	4.37	1.07	0.24	0.21	0.24	0.21	0.23	0.28	0.66	0.95
HD195019A	5842	4.32	1.27	0.09	-0.13	0.03	0.10	0.05	0.08	1.12	1.00
HD216437	5887	4.30	1.31	0.25	0.12	0.28	0.22	0.21	0.25	0.83	0.98
HD217014	5804	4.42	1.20	0.20	0.08	0.23	0.19	0.17	0.22	0.85	0.95
HD217107	5646	4.31	1.06	0.37	0.32	0.39	0.31	0.34	0.34	0.65	1.07
HD88133	5438	3.94	1.16	0.33	0.20	0.34	0.24	0.27	0.34	0.72	0.91

Table 6: Comparison sample stars from HARPS GTO survey.

Star	T <sub>eff</sub> K	log g km s <sup>-1</sup>	$\xi_t$ km s <sup>-1</sup>	[Fe/H]	[O/H]	[Ni/H]	[C/H]	[Mg/H]	[Si/H]	C/O	Mg/Si
HD283	5157.	4.51	0.45	-0.54	-0.17	-0.55	-0.47	-0.43	-0.47	0.33	1.17
HD361	5913.	4.60	1.00	-0.12	-0.11	-0.16	-0.16	-0.16	-0.12	0.59	0.98
HD870	5381.	4.42	0.79	-0.10	-0.12	-0.14	-0.15	-0.09	-0.12	0.62	1.15
HD967	5564.	4.51	0.79	-0.68	-0.17	-0.65	-0.40	-0.40	-0.45	0.39	1.20
HD1320	5679.	4.49	0.85	-0.27	-0.24	-0.31	-0.25	-0.26	-0.26	0.65	1.07
HD1388	5954.	4.41	1.13	-0.01	-0.09	-0.01	-0.07	-0.03	-0.01	0.69	1.02
HD1461	5765.	4.38	0.97	0.19	0.06	0.24	0.15	0.17	0.19	0.81	1.02
HD1581	5977.	4.51	1.12	-0.18	-0.20	-0.20	-0.20	-0.14	-0.15	0.66	1.10
HD2071	5719.	4.47	0.95	-0.09	-0.17	-0.11	-0.12	-0.11	-0.09	0.74	1.02
HD3569	5155.	4.54	0.60	-0.32	-0.15	-0.33	-0.26	-0.30	-0.28	0.51	1.02
HD3823	6022.	4.31	1.39	-0.28	-0.14	-0.29	-0.21	-0.19	-0.22	0.56	1.15
HD4307	5812.	4.10	1.22	-0.23	-0.18	-0.24	-0.18	-0.15	-0.17	0.66	1.12
HD4915	5658.	4.52	0.90	-0.21	-0.26	-0.24	-0.23	-0.19	-0.19	0.71	1.07
HD6348	5107.	4.51	0.07	-0.56	-0.35	-0.59	-0.28	-0.43	-0.48	0.78	1.20
HD6735	6082.	4.49	1.15	-0.06	-0.11	-0.10	-0.08	-0.09	-0.05	0.71	0.98
HD7134	5940.	4.41	1.17	-0.29	-0.16	-0.31	-0.26	-0.23	-0.25	0.52	1.12
HD7199	5386.	4.34	1.01	0.28	0.17	0.37	0.28	0.32	0.34	0.85	1.02
HD7449	6024.	4.51	1.11	-0.11	-0.11	-0.15	-0.16	-0.16	-0.11	0.59	0.95
HD8389A	5283.	4.37	1.06	0.34	0.35	0.44	0.37	0.36	0.40	0.69	0.98
HD8406	5726.	4.50	0.87	-0.10	-0.26	-0.14	-0.15	-0.11	-0.11	0.85	1.07
HD8638	5507.	4.43	0.74	-0.38	-0.17	-0.34	-0.19	-0.16	-0.21	0.63	1.20
HD8828	5403.	4.46	0.72	-0.16	-0.13	-0.16	-0.23	-0.16	-0.14	0.52	1.02
HD8859	5502.	4.41	0.77	-0.09	-0.09	-0.08	-0.10	-0.10	-0.08	0.65	1.02
HD8912	5211.	4.43	0.70	-0.07	-0.21	-0.08	-0.07	-0.10	-0.05	0.91	0.95
HD9782	6023.	4.42	1.09	0.09	0.05	0.10	0.07	0.02	0.07	0.69	0.95
HD9796	5179.	4.38	0.66	-0.25	-0.31	-0.25	-0.03	-0.20	-0.18	1.26	1.02
HD10002	5313.	4.40	0.82	0.17	0.09	0.20	0.22	0.16	0.20	0.89	0.98
HD10166	5221.	4.48	0.74	-0.39	-0.23	-0.41	-0.33	-0.38	-0.34	0.52	0.98
HD10180	5911.	4.39	1.11	0.08	0.03	0.11	0.09	0.08	0.10	0.76	1.02
HD10700	5310.	4.44	0.55	-0.52	-0.31	-0.50	-0.28	-0.31	-0.37	0.71	1.23
HD11226	6098.	4.35	1.28	0.04	0.04	0.06	0.09	0.01	0.06	0.74	0.95
HD11505	5752.	4.38	0.99	-0.22	0.01	-0.20	-0.09	-0.06	-0.12	0.52	1.23
HD12345	5395.	4.44	0.69	-0.21	-0.06	-0.21	-0.15	-0.18	-0.17	0.54	1.05
HD12387	5700.	4.39	0.93	-0.24	0.01	-0.21	-0.02	-0.07	-0.11	0.62	1.17
HD13060	5255.	4.34	0.82	0.02	-0.12	0.03	-0.06	0.03	0.03	0.76	1.07
HD13724	5868.	4.52	1.02	0.23	0.12	0.26	0.12	0.18	0.22	0.66	0.98
HD14374	5425.	4.48	0.81	-0.04	-0.11	-0.06	-0.07	-0.06	-0.03	0.72	1.00
HD14747	5516.	4.43	0.72	-0.39	-0.11	-0.37	-0.18	-0.19	-0.24	0.56	1.20
HD15337	5179.	4.39	0.70	0.06	0.21	0.09	0.09	0.06	0.09	0.50	1.00
HD16297	5422.	4.47	0.80	-0.01	-0.07	-0.03	-0.08	-0.07	-0.02	0.65	0.95
HD16714	5518.	4.42	0.76	-0.20	-0.13	-0.20	-0.16	-0.15	-0.16	0.62	1.10
HD18386	5457.	4.39	0.92	0.14	0.00	0.19	0.16	0.09	0.18	0.95	0.87
HD18719	5241.	4.41	0.92	-0.08	-0.03	-0.10	-0.04	-0.14	-0.04	0.65	0.85
HD19034	5477.	4.40	0.69	-0.48	-0.09	-0.45	-0.21	-0.18	-0.29	0.50	1.38

Table 7: Comparison sample stars from HARPS GTO survey.

Star	T <sub>eff</sub> K	log g	$\xi_t$ km s <sup>-1</sup>	[Fe/H]	[O/H]	[Ni/H]	[C/H]	[Mg/H]	[Si/H]	C/O	Mg/Si
HD19467	5720.	4.31	0.96	-0.14	0.01	-0.12	0.02	0.01	-0.06	0.68	1.26
HD20003	5494.	4.41	0.83	0.04	-0.02	0.05	0.02	0.01	0.04	0.72	1.00
HD20407	5866.	4.50	1.09	-0.44	-0.29	-0.44	-0.31	-0.38	-0.36	0.63	1.02
HD20619	5703.	4.51	0.92	-0.22	-0.27	-0.26	-0.25	-0.22	-0.21	0.69	1.05
HD20781	5256.	4.37	0.78	-0.11	-0.12	-0.13	-0.10	-0.10	-0.09	0.69	1.05
HD20794	5401.	4.40	0.67	-0.40	-0.17	-0.35	-0.14	-0.14	-0.21	0.71	1.26
HD20807	5866.	4.52	1.04	-0.23	-0.18	-0.24	-0.19	-0.20	-0.20	0.65	1.07
HD21019	5468.	3.93	1.05	-0.45	-0.23	-0.45	-0.40	-0.31	-0.37	0.45	1.23
HD21411	5473.	4.51	0.81	-0.26	-0.15	-0.30	-0.29	-0.26	-0.26	0.48	1.07
HD21693	5430.	4.37	0.76	0.00	-0.15	0.03	0.01	0.01	0.03	0.95	1.02
HD23249	5150.	3.89	1.01	0.13	0.22	0.16	0.14	0.19	0.16	0.55	1.15
HD23456	6178.	4.56	1.38	-0.32	-0.19	-0.34	-0.24	-0.30	-0.26	0.59	0.98
HD24892	5363.	3.99	0.88	-0.32	-0.10	-0.31	-0.20	-0.17	-0.21	0.52	1.17
HD25105	5316.	4.47	0.77	-0.15	-0.14	-0.17	-0.18	-0.17	-0.15	0.60	1.02
HD25120	5134.	4.47	0.87	-0.18	-0.17	-0.24	-0.09	-0.21	-0.18	0.79	1.00
HD25565	5212.	4.47	0.80	0.03	0.02	0.03	0.02	-0.01	0.04	0.66	0.95
HD25673	5136.	4.47	0.56	-0.50	-0.35	-0.50	-0.18	-0.44	-0.43	0.98	1.05
HD26965A	5153.	4.39	0.36	-0.31	-0.14	-0.26	-0.12	-0.10	-0.18	0.69	1.29
HD27063	5767.	4.44	0.94	0.05	-0.03	0.04	-0.04	0.01	0.03	0.65	1.02
HD28471	5745.	4.37	0.95	-0.05	-0.14	-0.06	-0.07	-0.04	-0.04	0.78	1.07
HD28701	5710.	4.41	0.95	-0.32	-0.12	-0.29	-0.12	-0.13	-0.16	0.66	1.15
HD28821	5660.	4.38	0.88	-0.12	-0.19	-0.15	-0.10	-0.06	-0.09	0.81	1.15
HD30278	5394.	4.39	0.72	-0.17	-0.05	-0.20	-0.15	-0.12	-0.15	0.52	1.15
HD30306	5529.	4.32	0.89	0.17	0.06	0.18	0.14	0.18	0.19	0.79	1.05
HD31527	5898.	4.45	1.09	-0.17	-0.22	-0.18	-0.17	-0.16	-0.16	0.74	1.07
HD31822	6042.	4.57	1.15	-0.19	-0.18	-0.24	-0.25	-0.19	-0.19	0.56	1.07
HD32724	5818.	4.26	1.14	-0.17	-0.08	-0.19	-0.14	-0.09	-0.12	0.58	1.15
HD33725	5274.	4.41	0.71	-0.17	-0.09	-0.16	-0.16	-0.16	-0.15	0.56	1.05
HD34449	5848.	4.50	0.92	-0.09	-0.08	-0.13	-0.13	-0.12	-0.11	0.59	1.05
HD34688	5169.	4.44	0.70	-0.20	-0.20	-0.20	-0.10	-0.19	-0.19	0.83	1.07
HD36108	5916.	4.33	1.21	-0.21	-0.14	-0.25	-0.19	-0.17	-0.19	0.59	1.12
HD36379	6030.	4.30	1.29	-0.17	-0.14	-0.18	-0.11	-0.12	-0.13	0.71	1.10
HD37962	5718.	4.48	0.84	-0.20	-0.12	-0.25	-0.25	-0.23	-0.19	0.49	0.98
HD37986	5507.	4.29	0.92	0.26	0.24	0.32	0.28	0.25	0.30	0.72	0.95
HD38277	5871.	4.34	1.10	-0.07	-0.07	-0.09	-0.06	-0.04	-0.07	0.68	1.15
HD38382	6082.	4.45	1.18	0.03	-0.18	0.00	-0.01	0.00	0.02	0.98	1.02
HD38858	5733.	4.51	0.94	-0.22	-0.23	-0.25	-0.21	-0.23	-0.21	0.69	1.02
HD38973	6016.	4.42	1.14	0.05	-0.07	0.06	0.05	0.01	0.05	0.87	0.98
HD39194	5205.	4.53	0.37	-0.61	-0.23	-0.57	-0.28	-0.42	-0.43	0.59	1.10
HD40105	5137.	3.85	0.97	0.06	0.11	0.09	0.06	0.09	0.10	0.59	1.05
HD40397	5527.	4.39	0.83	-0.13	0.10	-0.11	0.00	-0.02	-0.06	0.52	1.17
HD44120	6052.	4.25	1.31	0.12	0.05	0.14	0.08	0.10	0.13	0.71	1.00
HD44420	5818.	4.37	1.06	0.29	0.15	0.38	0.29	0.29	0.33	0.91	0.98
HD44447	5999.	4.37	1.26	-0.22	-0.11	-0.23	-0.16	-0.20	-0.18	0.59	1.02
HD44594	5840.	4.38	1.06	0.15	-0.02	0.18	0.10	0.13	0.15	0.87	1.02

Table 8: Comparison sample stars from HARPS GTO survey.

Star	T <sub>eff</sub> K	log g	$\xi_t$ km s <sup>-1</sup>	[Fe/H]	[O/H]	[Ni/H]	[C/H]	[Mg/H]	[Si/H]	C/O	Mg/Si
HD45184	5869.	4.47	1.03	0.04	-0.02	0.03	-0.02	0.03	0.04	0.66	1.05
HD45289	5717.	4.32	0.99	-0.02	0.10	-0.01	0.03	0.06	0.03	0.56	1.15
HD48611	5337.	4.51	0.69	-0.36	-0.31	-0.37	-0.31	-0.35	-0.31	0.66	0.98
HD50806	5633.	4.11	1.03	0.03	0.29	0.07	0.14	0.15	0.10	0.47	1.20
HD51608	5358.	4.36	0.73	-0.07	-0.11	-0.07	-0.07	-0.02	-0.02	0.72	1.07
HD55693	5914.	4.43	1.07	0.29	0.12	0.36	0.29	0.26	0.31	0.98	0.95
HD59468	5618.	4.39	0.88	0.03	-0.01	0.05	0.05	0.06	0.03	0.76	1.15
HD59711A	5722.	4.46	0.86	-0.12	-0.14	-0.13	-0.14	0.06	0.03	0.66	1.15
HD63765	5432.	4.42	0.82	-0.16	-0.21	-0.19	-0.22	-0.17	-0.15	0.65	1.02
HD65907A	5945.	4.52	1.05	-0.31	0.00	-0.27	-0.08	-0.05	-0.13	0.55	1.29
HD66221	5635.	4.40	0.92	0.17	0.03	0.22	0.14	0.17	0.18	0.85	1.05
HD67458	5891.	4.53	1.04	-0.16	-0.18	-0.18	-0.21	-0.16	-0.15	0.62	1.05
HD68607	5215.	4.41	0.82	0.07	-0.04	0.08	0.08	0.02	0.09	0.87	0.91
HD68978A	5965.	4.48	1.09	0.04	-0.08	0.04	0.00	0.00	0.04	0.79	0.98
HD69655	5961.	4.44	1.15	-0.18	-0.29	-0.19	-0.16	-0.16	-0.17	0.89	1.10
HD70889	6051.	4.49	1.13	0.11	0.00	0.09	-0.01	0.01	0.08	0.65	0.91
HD71334	5694.	4.37	0.95	-0.09	-0.11	-0.10	-0.12	-0.04	-0.08	0.65	1.17
HD71479	6026.	4.42	1.19	0.24	0.33	0.29	0.19	0.20	0.25	0.48	0.95
HD71835	5438.	4.39	0.79	-0.04	-0.17	-0.03	-0.04	-0.06	-0.02	0.89	0.98
HD72579	5449.	4.27	0.84	0.20	0.12	0.22	0.21	0.21	0.22	0.81	1.05
HD72673	5243.	4.46	0.60	-0.41	-0.33	-0.41	-0.25	-0.34	-0.36	0.79	1.12
HD72769	5640.	4.35	0.98	0.30	0.20	0.36	0.27	0.27	0.30	0.78	1.00
HD73121	6091.	4.30	1.34	0.09	0.01	0.10	0.06	0.07	0.12	0.74	0.95
HD73524	6017.	4.43	1.14	0.16	0.02	0.16	0.00	0.11	0.15	0.63	0.98
HD74014	5561.	4.33	0.90	0.22	0.05	0.27	0.23	0.20	0.26	1.00	0.93
HD76151	5788.	4.48	0.96	0.12	0.04	0.14	0.07	0.10	0.11	0.71	1.05
HD78429	5760.	4.33	1.01	0.09	0.27	0.07	0.08	0.08	0.09	0.43	1.05
HD78538	5786.	4.50	0.98	-0.03	-0.06	-0.08	-0.19	-0.08	-0.05	0.49	1.00
HD78558	5711.	4.36	0.99	-0.44	-0.08	-0.41	-0.15	-0.16	-0.23	0.56	1.26
HD78747	5778.	4.46	1.03	-0.67	-0.21	-0.65	-0.38	-0.38	-0.44	0.45	1.23
HD80883	5233.	4.44	0.80	-0.25	-0.32	-0.28	-0.29	-0.25	-0.22	0.71	1.00
HD81639	5522.	4.40	0.79	-0.17	-0.22	-0.16	-0.25	-0.11	-0.14	0.62	1.15
HD82516	5104.	4.46	0.71	0.01	0.07	0.04	0.18	-0.02	0.02	0.85	0.98
HD83529	5902.	4.35	1.11	-0.22	-0.20	-0.25	-0.24	-0.16	-0.20	0.60	1.17
HD85119	5425.	4.52	0.93	-0.20	-0.17	-0.26	-0.21	-0.24	-0.20	0.60	0.98
HD85390	5186.	4.41	0.75	-0.07	-0.13	-0.06	0.04	-0.08	-0.03	0.98	0.95
HD86171	5400.	4.47	0.81	-0.25	-0.34	-0.29	-0.32	-0.24	-0.22	0.69	1.02
HD88218	5878.	4.16	1.23	-0.14	-0.12	-0.15	-0.08	-0.10	-0.11	0.72	1.10
HD88656	5150.	4.44	0.81	-0.11	-0.21	-0.14	-0.18	-0.16	-0.10	0.71	0.93
HD88742	5981.	4.52	1.07	-0.02	-0.10	-0.05	-0.04	-0.08	-0.03	0.76	0.95
HD89454	5728.	4.47	0.96	0.12	-0.03	0.12	0.01	0.07	0.10	0.72	1.00
HD90156	5599.	4.48	0.86	-0.24	-0.24	-0.25	-0.30	-0.18	-0.21	0.58	1.15
HD90711	5444.	4.40	0.92	0.24	0.16	0.31	0.23	0.24	0.27	0.78	1.00
HD90812	5164.	4.48	0.64	-0.36	-0.28	-0.35	-0.28	-0.30	-0.30	0.66	1.07
HD92588	5199.	3.79	1.01	0.04	0.08	0.04	-0.05	0.05	0.05	0.49	1.07

Table 9: Comparison sample stars from HARPS GTO survey.

Star	T <sub>eff</sub> K	log g km s <sup>-1</sup>	$\xi_t$ km s <sup>-1</sup>	[Fe/H]	[O/H]	[Ni/H]	[C/H]	[Mg/H]	[Si/H]	C/O	Mg/Si
HD92719	5824.	4.51	0.96	-0.10	-0.16	-0.13	-0.18	-0.12	-0.10	0.63	1.02
HD93385	5977.	4.42	1.14	0.02	-0.03	0.03	-0.01	0.00	0.02	0.69	1.02
HD94151	5583.	4.38	0.83	0.04	-0.10	0.06	0.03	0.03	0.05	0.89	1.02
HD95456	6276.	4.35	1.40	0.16	0.10	0.15	0.09	0.10	0.15	0.65	0.95
HD95521	5773.	4.49	0.96	-0.15	-0.16	-0.18	-0.17	-0.17	-0.15	0.65	1.02
HD96423	5711.	4.35	0.98	0.10	-0.01	0.13	0.07	0.12	0.11	0.79	1.10
HD96700	5845.	4.39	1.04	-0.18	-0.10	-0.21	-0.15	-0.15	-0.16	0.59	1.10
HD97037	5883.	4.34	1.13	-0.07	-0.10	-0.09	-0.08	-0.06	-0.05	0.69	1.05
HD97343	5410.	4.39	0.82	-0.06	-0.04	-0.06	-0.06	0.03	-0.01	0.63	1.17
HD97998	5716.	4.57	0.85	-0.42	-0.24	-0.44	-0.38	-0.36	-0.37	0.48	1.10
HD98281	5381.	4.42	0.64	-0.26	-0.25	-0.26	-0.26	-0.19	-0.21	0.65	1.12
HD98356	5322.	4.41	0.84	0.10	0.03	0.13	0.09	0.08	0.12	0.76	0.98
HD100508	5449.	4.42	0.86	0.39	0.25	0.49	0.31	0.37	0.41	0.76	0.98
HD102365	5629.	4.44	0.91	-0.29	-0.11	-0.30	-0.17	-0.23	-0.19	0.58	0.98
HD102438	5560.	4.41	0.84	-0.29	-0.26	-0.30	-0.24	-0.22	-0.24	0.69	1.12
HD104263	5477.	4.34	0.81	0.02	0.01	0.04	0.09	0.08	0.06	0.79	1.12
HD104982	5692.	4.44	0.91	-0.19	-0.24	-0.20	-0.18	-0.15	-0.17	0.76	1.12
HD105837	5907.	4.54	1.14	-0.51	-0.37	-0.51	-0.13	-0.45	-0.45	1.15	1.07
HD106116	5680.	4.39	0.91	0.14	0.12	0.17	0.09	0.11	0.14	0.62	1.00
HD108309	5775.	4.23	1.08	0.12	0.10	0.13	0.15	0.13	0.13	0.74	1.07
HD109200	5134.	4.51	0.68	-0.31	-0.20	-0.33	-0.19	-0.27	-0.28	0.68	1.10
HD109409	5886.	4.16	1.24	0.33	0.22	0.40	0.24	0.24	0.32	0.69	0.89
HD111031	5801.	4.39	1.05	0.27	0.21	0.34	0.24	0.23	0.27	0.71	0.98
HD112540	5523.	4.52	0.74	-0.17	-0.26	-0.20	-0.22	-0.20	-0.17	0.72	1.00
HD114613	5729.	3.97	1.18	0.19	0.10	0.24	0.13	0.17	0.21	0.71	0.98
HD114747	5172.	4.44	0.98	0.21	0.18	0.30	0.35	0.21	0.28	0.98	0.91
HD114853	5705.	4.44	0.92	-0.23	0.01	-0.25	-0.25	-0.19	-0.20	0.36	1.10
HD115585	5711.	4.27	1.14	0.35	0.22	0.40	0.34	0.33	0.35	0.87	1.02
HD115617	5558.	4.36	0.81	-0.02	-0.08	-0.01	-0.11	0.00	0.00	0.62	1.07
HD115674	5649.	4.48	0.85	-0.17	-0.28	-0.20	-0.22	-0.22	-0.17	0.76	0.95
HD117105	5889.	4.41	1.13	-0.29	-0.28	-0.32	-0.23	-0.19	-0.22	0.74	1.15
HD119638	6069.	4.42	1.22	-0.15	-0.11	-0.17	-0.13	-0.16	-0.12	0.63	0.98
HD119782	5160.	4.44	0.79	-0.07	-0.10	-0.07	0.00	-0.10	-0.05	0.83	0.95
HD122862	5982.	4.23	1.29	-0.12	-0.09	-0.12	-0.08	-0.12	-0.09	0.68	1.00
HD123265	5338.	4.29	0.85	0.19	0.14	0.22	0.27	0.27	0.27	0.89	1.07
HD124106	5106.	4.49	0.80	-0.17	-0.17	-0.20	-0.18	-0.23	-0.14	0.65	0.87
HD124292	5443.	4.37	0.77	-0.13	-0.12	-0.12	-0.07	-0.07	-0.09	0.74	1.12
HD124364	5584.	4.48	0.83	-0.27	-0.28	-0.31	-0.31	-0.26	-0.26	0.62	1.07
HD125184	5680.	4.10	1.13	0.27	0.15	0.28	0.18	0.25	0.27	0.71	1.02
HD125455	5162.	4.52	0.70	-0.18	-0.18	-0.18	-0.06	-0.18	-0.17	0.87	1.05
HD125881	6036.	4.49	1.10	0.06	-0.05	0.05	-0.01	0.00	0.05	0.72	0.95
HD126525	5638.	4.37	0.90	-0.10	-0.11	-0.08	-0.07	-0.08	-0.08	0.72	1.07
HD128674	5551.	4.50	0.71	-0.38	-0.35	-0.38	-0.34	-0.33	-0.32	0.68	1.05
HD132648	5418.	4.49	0.69	-0.37	-0.38	-0.38	-0.35	-0.33	-0.34	0.71	1.10
HD134060	5966.	4.43	1.10	0.14	-0.04	0.15	0.07	0.11	0.12	0.85	1.05

Table 10: Comparison sample stars from HARPS GTO survey.

Star	T <sub>eff</sub> K	log g km s <sup>-1</sup>	$\xi_t$ km s <sup>-1</sup>	[Fe/H]	[O/H]	[Ni/H]	[C/H]	[Mg/H]	[Si/H]	C/O	Mg/Si
HD134606	5633.	4.38	1.00	0.27	0.21	0.33	0.27	0.26	0.30	0.76	0.98
HD134664	5865.	4.52	0.99	0.10	-0.05	0.09	-0.02	0.03	0.08	0.71	0.95
HD136894	5412.	4.36	0.75	-0.10	-0.11	-0.13	-0.12	-0.11	-0.11	0.65	1.07
HD137388	5240.	4.42	0.93	0.18	0.26	0.25	0.28	0.20	0.24	0.69	0.98
HD138549	5582.	4.44	0.87	0.00	-0.10	0.03	0.02	-0.02	0.01	0.87	1.00
HD140901	5610.	4.46	0.90	0.09	-0.04	0.11	0.05	0.05	0.08	0.81	1.00
HD143114	5775.	4.39	0.92	-0.41	-0.12	-0.39	-0.24	-0.22	-0.26	0.50	1.17
HD144585	5914.	4.35	1.15	0.33	0.22	0.39	0.20	0.30	0.33	0.63	1.00
HD145598	5417.	4.48	0.59	-0.78	-0.44	-0.75	-0.52	-0.46	-0.54	0.55	1.29
HD145666	5958.	4.53	1.04	-0.04	-0.21	-0.08	-0.11	-0.09	-0.06	0.83	1.00
HD145809	5778.	4.15	1.14	-0.25	-0.05	-0.29	-0.20	-0.16	-0.21	0.47	1.20
HD146233	5818.	4.45	1.00	0.04	-0.04	0.04	-0.03	0.03	0.04	0.68	1.05
HD147512	5530.	4.40	0.81	-0.08	-0.09	-0.06	-0.04	-0.04	-0.06	0.74	1.12
HD151504	5457.	4.36	0.87	0.06	0.16	0.07	0.14	0.10	0.10	0.63	1.07
HD154088	5374.	4.37	0.85	0.28	0.19	0.35	0.29	0.25	0.30	0.83	0.95
HD154962	5827.	4.17	1.22	0.32	0.25	0.39	0.28	0.30	0.32	0.71	1.02
HD157172	5451.	4.39	0.77	0.11	-0.05	0.15	0.11	0.10	0.12	0.95	1.02
HD157347	5676.	4.38	0.91	0.02	-0.10	0.03	-0.03	0.00	0.02	0.78	1.02
HD161098	5560.	4.46	0.79	-0.27	-0.23	-0.29	-0.29	-0.26	-0.25	0.58	1.05
HD161612	5616.	4.45	0.88	0.16	0.05	0.17	0.10	0.14	0.16	0.74	1.02
HD162236	5343.	4.43	0.82	-0.12	-0.13	-0.13	-0.14	-0.15	-0.10	0.65	0.95
HD162396	6090.	4.27	1.43	-0.35	-0.23	-0.33	-0.26	-0.25	-0.27	0.62	1.12
HD165920	5339.	4.39	0.79	0.29	0.44	0.32	0.49	0.23	0.31	0.74	0.89
HD166724	5127.	4.43	0.79	-0.09	-0.20	-0.10	0.01	-0.12	-0.10	1.07	1.02
HD167359	5348.	4.46	0.67	-0.19	-0.17	-0.22	-0.26	-0.19	-0.17	0.54	1.02
HD168871	5983.	4.42	1.17	-0.09	-0.15	-0.10	-0.07	-0.09	-0.07	0.79	1.02
HD171665	5655.	4.41	0.89	-0.05	-0.14	-0.05	-0.09	-0.07	-0.03	0.74	0.98
HD171990	6045.	4.14	1.40	0.06	0.09	0.08	0.08	0.06	0.08	0.65	1.02
HD172513	5500.	4.41	0.79	-0.05	-0.22	-0.07	-0.12	-0.07	-0.04	0.83	1.00
HD174545	5216.	4.40	0.88	0.22	0.12	0.28	0.30	0.21	0.25	1.00	0.98
HD176157	5181.	4.41	0.92	-0.16	-0.33	-0.16	-0.06	-0.13	-0.13	1.23	1.07
HD177409	5898.	4.49	0.99	-0.04	-0.16	-0.07	-0.13	-0.05	-0.04	0.71	1.05
HD177565	5627.	4.39	0.91	0.08	0.16	0.11	0.06	0.06	0.09	0.52	1.00
HD177758	5862.	4.41	1.11	-0.58	-0.26	-0.56	-0.34	-0.37	-0.39	0.55	1.12
HD180409	6013.	4.52	1.16	-0.17	-0.17	-0.19	-0.15	-0.17	-0.16	0.69	1.05
HD183658	5803.	4.40	1.00	0.03	-0.32	0.05	0.03	0.01	0.03	1.48	1.02
HD185615	5570.	4.34	0.84	0.08	0.12	0.12	0.16	0.11	0.12	0.72	1.05
HD189567	5726.	4.41	0.95	-0.24	-0.18	-0.26	-0.16	-0.15	-0.20	0.69	1.20
HD189625	5846.	4.43	1.03	0.18	0.31	0.20	0.08	0.13	0.19	0.39	0.93
HD190248	5604.	4.26	0.99	0.33	0.30	0.37	0.30	0.30	0.35	0.66	0.95
HD192031	5215.	4.39	0.04	-0.84	-0.48	-0.85	-0.50	-0.57	-0.59	0.63	1.12
HD192117	5479.	4.48	0.75	-0.04	-0.31	-0.07	-0.02	-0.09	-0.07	1.29	1.02
HD192310	5166.	4.51	0.97	-0.04	-0.08	-0.01	0.14	-0.01	-0.03	1.10	1.12
HD193193	5979.	4.40	1.15	-0.05	0.04	-0.05	-0.03	-0.05	-0.04	0.56	1.05
HD195564	5676.	4.03	1.11	0.06	0.02	0.05	0.04	0.09	0.06	0.69	1.15

Table 11: Comparison sample stars from HARPS GTO survey.

Star	T <sub>eff</sub> K	log g km s <sup>-1</sup>	$\xi_t$ km s <sup>-1</sup>	[Fe/H]	[O/H]	[Ni/H]	[C/H]	[Mg/H]	[Si/H]	C/O	Mg/Si
HD196761	5415.	4.43	0.76	-0.31	-0.39	-0.31	-0.26	-0.29	-0.27	0.89	1.02
HD196800	6010.	4.37	1.17	0.19	0.19	0.22	0.16	0.14	0.17	0.62	1.00
HD197210	5577.	4.42	0.86	-0.03	-0.17	-0.05	-0.14	-0.06	-0.03	0.71	1.00
HD197823	5396.	4.41	0.82	0.12	-0.06	0.15	0.11	0.08	0.14	0.98	0.93
HD198075	5846.	4.56	0.95	-0.24	-0.10	-0.28	-0.31	-0.25	-0.25	0.41	1.07
HD199288	5765.	4.50	1.00	-0.63	-0.29	-0.63	-0.39	-0.43	-0.46	0.52	1.15
HD199960	5973.	4.39	1.13	0.28	0.23	0.34	0.23	0.24	0.29	0.66	0.95
HD202605	5658.	4.49	1.02	0.18	0.13	0.19	0.11	0.12	0.17	0.63	0.95
HD203384	5586.	4.40	0.90	0.26	0.19	0.31	0.23	0.24	0.26	0.72	1.02
HD203432	5645.	4.39	0.98	0.29	0.16	0.36	0.22	0.29	0.29	0.76	1.07
HD204385	6033.	4.44	1.15	0.07	0.00	0.08	0.05	0.05	0.07	0.74	1.02
HD205536	5442.	4.38	0.77	-0.05	-0.09	-0.03	-0.09	-0.01	-0.01	0.66	1.07
HD206163	5519.	4.43	0.94	0.01	-0.07	-0.03	-0.18	-0.05	0.01	0.51	0.93
HD206172	5608.	4.49	0.77	-0.24	-0.19	-0.28	-0.23	-0.26	-0.23	0.60	1.00
HD207129	5937.	4.49	1.06	0.00	-0.08	-0.02	-0.09	-0.02	-0.01	0.65	1.05
HD207583	5534.	4.46	0.99	0.01	-0.58	-0.03	-0.21	-0.05	-0.02	1.55	1.00
HD207700	5666.	4.29	0.98	0.04	0.09	0.07	0.14	0.13	0.11	0.74	1.12
HD208272	5199.	4.42	0.99	-0.08	-0.12	-0.11	0.02	-0.11	-0.04	0.91	0.91
HD208704	5826.	4.38	1.04	-0.09	-0.04	-0.11	-0.09	-0.10	-0.08	0.59	1.02
HD209742	5137.	4.49	0.79	-0.16	-0.48	-0.16	-0.04	-0.19	-0.15	1.82	0.98
HD210918	5755.	4.35	0.99	-0.09	-0.02	-0.11	-0.03	-0.04	-0.07	0.65	1.15
HD211415	5850.	4.39	0.99	-0.21	-0.22	-0.23	-0.20	-0.17	-0.19	0.69	1.12
HD212580	5155.	4.44	0.85	-0.11	-0.13	-0.14	0.01	-0.16	-0.12	0.91	0.98
HD212708	5681.	4.35	0.99	0.27	0.21	0.33	0.24	0.24	0.26	0.71	1.02
HD213575	5671.	4.18	1.02	-0.15	0.05	-0.12	0.01	0.05	-0.03	0.60	1.29
HD213628	5555.	4.44	0.82	0.01	-0.03	0.03	0.02	-0.02	0.02	0.74	0.98
HD214759	5461.	4.37	0.85	0.18	0.06	0.23	0.10	0.16	0.17	0.72	1.05
HD215456	5789.	4.10	1.19	-0.09	-0.20	-0.11	-0.08	-0.06	-0.06	0.87	1.07
HD216777	5623.	4.51	0.81	-0.38	-0.33	-0.39	-0.36	-0.30	-0.33	0.62	1.15
HD219077	5362.	4.00	0.92	-0.13	-0.05	-0.14	-0.13	-0.05	-0.08	0.55	1.15
HD219249	5482.	4.50	0.74	-0.40	-0.44	-0.41	-0.34	-0.34	-0.36	0.83	1.12
HD220256	5144.	4.41	0.47	-0.10	-0.05	-0.07	0.11	-0.04	-0.04	0.95	1.07
HD220367	6128.	4.37	1.34	-0.21	-0.16	-0.23	-0.18	-0.19	-0.16	0.63	1.00
HD220507	5698.	4.29	1.01	0.01	0.12	0.03	0.11	0.11	0.05	0.65	1.23
HD221146	5876.	4.27	1.09	0.08	0.01	0.11	0.09	0.11	0.11	0.79	1.07
HD221356	6112.	4.53	1.12	-0.20	-0.06	-0.22	-0.29	-0.18	-0.19	0.39	1.10
HD221420	5847.	4.03	1.28	0.33	0.21	0.42	0.26	0.37	0.36	0.74	1.10
HD222335	5271.	4.49	0.83	-0.20	-0.19	-0.22	-0.22	-0.20	-0.17	0.62	1.00
HD222422	5475.	4.46	0.73	-0.12	-0.18	-0.15	-0.28	-0.11	-0.11	0.52	1.07
HD222595	5648.	4.46	0.88	0.01	-0.05	0.02	-0.03	-0.01	0.02	0.69	1.00
HD222669	5894.	4.46	1.01	0.05	-0.03	0.05	-0.01	0.03	0.03	0.69	1.07
HD223171	5841.	4.20	1.12	0.12	0.11	0.14	0.10	0.12	0.11	0.65	1.10
HD223282	5328.	4.49	0.60	-0.41	-0.36	-0.44	-0.31	-0.38	-0.37	0.74	1.05
HD224393	5774.	4.54	0.84	-0.38	-0.34	-0.41	-0.42	-0.33	-0.36	0.55	1.15
HD224619	5436.	4.39	0.79	-0.20	-0.18	-0.20	-0.20	-0.14	-0.16	0.63	1.12
HD224789	5185.	4.44	1.05	-0.03	-0.01	-0.03	0.06	-0.07	0.01	0.78	0.89

## REFERENCES

- Andersson, H. & Edvardsson, D. 1994, A&A, 290, 590
- Anders, E. & Grevesse, N. 1989, Geochim, Cosmochim. Acta, 53, 197
- Allende Prieto, C., Lambert, D. L. & Asplund, M. 2001, ApJ, 556, 63
- Beirão, P., Santos, N. C., Israelian, G., & Mayor, M. 2005, A&A, 438, 251
- Bensby, T., Feltzing, S. & Lundström, I. 2004, A&A, 415, 155
- Bodaghee, A., Santos, N. C., Israelian, G., & Mayor, M. 2003, A&A, 404, 715
- Bond, J. C., Tinney, C. G., Butler, R. P., Jones, H. R. A., Marcy, G. W., Penny, A. J., & Carter, B. D. 2006, MNRAS, 370, 163
- Bond, J. C., et al. 2008, ApJ, 682, 1234
- Bond, J. C.; Lauretta, D. S. & O'Brien, D. P. 2010a, Icarus, 205, 321
- Bond, J. C.; O'Brien, D. P. & Lauretta, D. S. 2010b, ApJ, 715, 1050
- Boss, A. P. 1997, Science, 276, 1836
- Boss, A. P. 2002, ApJ, 567, 149
- Ecuvillon, A.; Israelian, G.; Santos, N. C.; Mayor, M.; Villar, V. & Bihain, G. 2004, A&A, 426, 619
- Ecuvillon, A.; Israelian, G.; Santos, N. C.; Shchukina, N. G.; Mayor, M. & Rebolo, R. 2006a, A&A, 445, 633
- Ecuvillon, A.; Israelian, G.; Santos, N. C.; Mayor, M. & Gilli, G. 2006b, A&A, 449, 809
- Edvardsson, B., Andersen, J., Gustafsson, B. et al. 1993, A&A, 275, 101
- Gilli, G.; Israelian, G.; Ecuvillon, A.; Santos, N. C. & Mayor, M. 2006, A&A, 449, 723
- Gonzalez, G. 1998, A&A, 334, 221
- Gonzalez, G. & Laws, C. 2000, AJ, 119, 390
- Gonzalez, G., Laws, C., Tyagi, S. & Reddy, B. E. 2001, AJ, 121, 432
- Gonzalez, G., & Laws, C. 2007, MNRAS, 378, 1141
- González Hernández, J.I., Israelian, G., Santos, N. C., Sousa, S. G., Delgado Mena, E., Neves, V. & Udry, S. 2010, ApJ, 720, 1592
- Gray, D. F., Tycner, C., & Brown, K. 2000, PASP, 112, 328
- Guillot, T., Santos, N. C., Pont, F., Iro, N., Melo, C. & Ribas, I. 2006, A&A, 453, L21
- Fischer, D.A. & Valenti, J. 2005, AJ, 622, 1102
- Kiselman, d. 1991, A&A, 245, L9
- Kupka, F., Piskunov, N., Ryabchikova, T. A., Stempels, H. C. & Weiss, W. W. 1999 A&AS, 138, 119
- Kurucz, R. L. 1993, ATLAS9 Stellar Atmospheres Programs and 2 kms<sup>-1</sup> Grid (CD-ROM, Smithsonian Astrophysical Observatory, Cambridge)
- Mayor, M. & Queloz, D. 1995, Nature, 378, 355
- Lambert, D. L. 1978, MNRAS, 182, 249
- Mayor, M., Queloz, D. et al. 2003, The Messenger, 114, 20
- Mordasini, C., Alibert, Y., Benz, W., & Naef, D. 2009, A&A, 501, 1161
- Nissen, P. E. & Edvardsson, B. 1992, A&A, 261, 255
- Nissen, P. E.; Gustafsson, B., Edvardsson, B. & Gilmore, G. 1994, A&A, 285, 440
- Nissen, P. E.; Primas, F.; Asplund, M. & Lambert, D. L. 2002, A&A, 390, 235
- Neves, V., Santos, N. C., Sousa, S. G., Correia, A. C. M. & Israelian, G. 2009, A&A, 497, 563
- Pollack, J. B., Hubickyj, O., Bodenheimer, P., Lissauer, J. J., Podolak, M. & Greenzweig, Y. 1996, Icarus, 124, 62
- Robinson, S. E., Laughlin, G., Bodenheimer, P., & Fischer, D. 2006, ApJ, 643, 484

Sadakane, K., Ohkubo, M., Takeda, Y., Sato, B.  
Kambe, E. & Aoki, W. 2002, PASJ, 54, 911

Santos, N. C., Israelian, G. & Mayor, M. 2000,  
A&A, 363, 228

Santos, N. C., Israelian, G. & Mayor, M. 2001,  
A&A, 373, 1019 A&A, 415, 1153

Santos, N. C., Israelian, G., & Mayor, M. 2004,  
A&A, 415, 1153

Santos, N. C., Israelian, G., Mayor, M., Bento,  
J. P., Almeida, P. C., Sousa, S. G., & Ecuvillon,  
A., 2005, A&A, 437, 1127

Sousa, S. G.; Santos, N. C.; Israelian, G.; Mayor,  
M. & Monteiro, M. J. P. F. G. 2007, A&A, 469,  
783

Sousa, S.G., Santos, N.C., Mayor, M., Udry, S.,  
Casagrande, L., Israelian, G., Pepe, F., Queloz,  
D. & Monteiro, F.G. 2008, A&A, 487, 373

Sneden, C. 1973 Ph.D Thesis, University of Texas.

Takeda, Y. 2007, PASJ, 59, 335